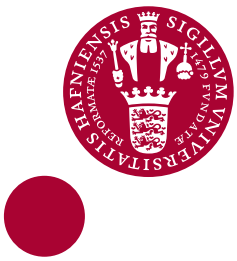

Atmospheric impacts of sea ice decline in CO2 induced global warming

Cvijanovic, Ivana; Caldeira, Ken

Published in:
Climate Dynamics

DOI:
10.1007/s00382-015-2489-1

Publication date:
2015

Document version
Publisher's PDF, also known as Version of record

Clim Dyn (2015) 44:1173–1186
DOI 10.1007/s00382-015-2489-1

Atmospheric impacts of sea ice decline in CO_2 induced global warming

Ivana Cvijanovic · Ken Caldeira

Received: 7 September 2013 / Accepted: 14 January 2015 / Published online: 7 February 2015

Abstract Changes in sea ice cover have important consequences for both Earth's energy budget and atmospheric dynamics. Sea ice acts as a positive feedback in the climate system, amplifying effects of radiative forcing while also affecting the meridional and interhemispheric temperature gradients that can impact mid- and low latitude atmospheric circulation. In this study, we partition and evaluate the effects of changing sea ice cover on global warming using a set of simulations with active and suppressed sea ice response. Two aspects of CO_2-induced sea ice changes are investigated: (1) the effect of changing sea ice cover on global and local temperature changes; and (2) the impact of sea ice loss on atmospheric circulation and extreme weather events. We find that in the absence of sea ice decline, global temperature response decreases by 21–37 %, depending on the sea ice treatment and the CO_2 forcing applied. Weakened global warming in the absence of changes in sea ice cover is not only due to a decreased high latitude warming but is also a consequence of a weaker tropical warming. In the northern midlatitudes, sea ice decline affects the magnitude and sign of zonal wind response to global warming in the winter and autumn seasons. Presence or absence of sea ice cover impacts the intensity and frequency of winter extreme precipitation and temperature events (temperature minima, number of heavy precipitation days and number of ice days). For some of the analyzed extreme weather indices, the difference between the responses with and without sea ice decline is eliminated when taking into account the amplifying effect of sea ice loss on hemispheric warming. However, in other cases, we find the influence of higher order factors, exerting weaker but opposing effects than those expected from the global temperature increase.

Keywords Global warming · Sea ice decline · Atmospheric circulation · Extreme weather

I. Cvijanovic (✉) · K. Caldeira
Department of Global Ecology, Carnegie Institution for Science, 260 Panama St., Stanford, CA 94305, USA
e-mail: ivanacv@carnegiescience.edu

I. Cvijanovic
Centre for Ice and Climate, Niels Bohr Institute, University of Copenhagen, Copenhagen, Denmark

1 Introduction

In recent decades, temperatures in the high northern latitudes have increased more than in any other area in the world, with the Arctic temperature increase being nearly double the global average change (Solomon 2006; Serreze and Francis 2006; IPCC 2007). Amplified warming in the Arctic has been predicted in several generations of climate models (Manabe and Stouffer 1980; Hansen et al. 1984; Washington and Meehl 1996; Holland and Bitz 2003; Murray and Walsh 2005; Masson-Delmotte et al. 2005). The amplification is a consequence of a combination of several factors, with retreating sea ice cover playing a central role (Chapman and Walsh 2007; Serreze et al. 2009; Screen and Simmonds 2010). Sea ice loss affects Arctic temperatures through the surface albedo feedback (Budyko 1969; Sellers 1969; Robock 1983; Hall 2004) and by affecting the atmosphere–ocean heat exchange through 'ice insulation feedback' (Holland et al. 2001, 2006a; Serreze et al. 2009; Jackson et al. 2010; Screen and Simmonds 2010; Overland et al. 2011). Other important factors contributing to amplification of high latitude warming include changes in atmospheric sensible and latent heat transport (Alexeev et al. 2005; Langen and Alexeev 2007; Graversen et al. 2008; Graversen and Wang 2009; Alexeev and Jackson 2012),

cloud and water vapor radiative forcing (Vavrus and Harrison 2003; Graversen and Wang 2009; Kapsch et al. 2013) and changes in ocean heat transport (Polyakov 2005; Mahlstein and Knutti 2011; Stroeve et al. 2011).

Climate model projections show that future abrupt transitions in Arctic sea ice extent are 'quite likely' (Holland et al. 2006b) with seasonally ice free conditions in the Arctic expected in the next few decades (Wang and Overland 2012, 2013; Stroeve et al. 2012). This is supported by another record minimum in Arctic sea ice extent observed in 2012, which was 49 % below the 1979–2000 average [according to National Snow and Ice Data Center (NSIDC), NSDIC 2012].

High latitude temperature changes have been shown to exhibit remote effects, one of which is an influence on the spatial distribution of tropical precipitation (Chiang and Bitz 2005; Broccoli et al. 2006). A number of modeling and observational studies suggest a link between Arctic sea ice loss and changes in midlatitude atmospheric circulation and weather (Francis et al. 2009; Overland and Wang 2010; Petoukhov and Semenov 2010; Deser et al. 2010; Liu et al. 2012; Blüthgen et al. 2012; Screen and Simmonds 2013; Screen et al. 2013; Peings and Magnusdottir 2014). Francis and Vavrus (2012) argue that amplified Arctic warming is one of the causes behind the increased frequency and intensity of extreme weather events with global warming. In their view, Arctic amplification contributes to a slower progression and increased amplitude of Rossby waves, which is associated with persistent weather patterns ('blocking events'). Screen and Simmonds (2013) suggest a more complex relation between Arctic warming and planetary waves by showing that such a link (and its implications for midlatitude weather) is sensitive to different measures of atmospheric planetary wave amplitude. A recent study based on reanalysis data (Barnes 2013) finds no statistically significant increase in the frequency of blocking events. Studies based on observational data have not yet been able to confirm a statistically significant relation between the amplification of Arctic warming and extreme weather changes (Hopsch et al. 2012).

Revisiting the role of sea ice in global warming by partitioning the responses arising from changes in sea ice cover only could help the ongoing discussion on the links between Arctic warming, midlatitude atmospheric circulation changes and extreme weather events. Several recent studies (Deser et al. 2010; Screen et al. 2013, Screen 2013; Peings and Magnusdottir 2014), have treated sea ice changes as a forcing on the climate system and investigated its effects on atmospheric circulation patterns in simulations with prescribed sea ice cover and sea surface temperatures. These studies have made an important contribution to understanding the atmospheric impacts of Arctic sea ice decline. However, prescribing the sea surface temperatures (SSTs) may eliminate some of the teleconnections arising from the sea ice changes—those that require atmosphere–surface ocean interaction (i.e. sea surface temperature changes) for their propagation. For example, Cvijanovic and Chiang (2013) demonstrated that tropical precipitation shifts due to high northern latitude cooling are not possible when the tropical SSTs are fixed. Yet, it is not just the information on tropical circulation changes that is lost when disabling the sea ice changes—the absence of tropical response further affects atmospheric teleconnections from the tropics to the high northern latitudes (Cvijanovic et al. 2013; Ding et al. 2014). The importance of SST changes for the propagation of global atmospheric teleconnections (Cvijanovic and Chiang 2013; Hsieh et al. 2013) highlights the substantial difference between the approaches using prescribed SST model configurations (testing the atmospheric response to a given sea ice geometry and SST distribution) and prescribed ice configurations (testing the atmospheric response to a given sea ice geometry only).

The aim of the current study is to isolate the component of global warming originating from the sea ice loss. The evaluated sea ice impacts are an integral result of direct effects of sea ice changes (ice albedo feedback, atmosphere–ocean insulation effects, etc.) as well as sea ice triggered feedbacks and effects (cloud responses, atmospheric circulation changes etc.). Using two different methods to eliminate the sea ice response, we isolate the components of global warming and atmospheric circulation changes that are driven by sea ice loss. We investigate the effects of CO_2 induced sea ice loss on global and local temperature changes, climate sensitivity, atmospheric circulation responses and atmospheric heat transport (AHT) partitioning as well as on the occurrence of extreme weather events. In our simulations SSTs are allowed to respond to changing climatic conditions, thus enabling the interactions with remote areas and propagation of atmospheric teleconnections globally.

The paper is organized as follows: model setup and experimental design are described in Sect. 2; results are presented in Sect. 3 while their implications are discussed in Sect. 4. Conclusions are given in Sect. 5.

2 Model configuration and experiment description

In our study, we employ the National Center for Atmospheric Research's Community Earth System Model (CESM) version 1.0.4 in a slab ocean mode (Gent et al. 2011; Danabasoglu and Gent 2009). This configuration incorporates the Community Atmosphere Model version 4 (CAM4, Neale et al. 2013), Community Land Model version 4 (CLM4, Lawrence et al. 2011) and Los Alamos Sea Ice Model version 4 (Community Ice CodeE 4—CICE4,

Hunke and Lipscomb 2008) coupled to a mixed layer (slab) ocean. Ocean dynamics are not accounted for in a slab ocean model. Instead the data necessary to run the mixed layer ocean model (prescribed ocean heat flux (often called 'q-flux'), salinity, temperature and velocity fields) are derived from the preindustrial (fully coupled) CESM simulation using the full-depth ocean. In the configuration applied, the atmosphere and land model are run using a 1.9 × 2.5 (latitude × longitude) finite volume grid with 26 atmospheric levels in the vertical dimension. The ice and ocean models are defined on a 1° displaced pole grid (gx1v6). In all simulations the solar insolation and orbital parameters are set to preindustrial values (CH_4 = 791.6 ppb, CO_2 = 284.7 ppm, N_2O = 275.7 ppb). In the forced runs, CO_2 forcing is applied instantaneously and equals 2, 4, 6 or 8 times the value of the control simulation.

In addition to the standard slab ocean simulations (that we refer to as 'active ice'), we performed two additional sets of slab ocean simulations in which the sea ice response has been disabled (namely 'zero ice' and 'prescribed ice'). The only difference between the three sets of simulations is the treatment of sea ice. With the active sea ice treatment, the model produces sea ice according to the model physics. In the zero ice setup, ocean temperatures are allowed to fall below freezing point and thus there is no sea ice formation at any location at any time. The prescribed ice setup could be viewed as a "hybrid" between: (1) the standard slab ocean model with interactive sea ice and interactive SSTs and (2) the data ocean model with prescribed sea ice and prescribed SSTs. Thirty years of monthly sea ice fractions derived from the control active ice simulation were used to force the sea ice changes in the prescribed ice simulations. Ice thickness is set uniformly to 1 m in the Northern and 2 m in the Southern Hemisphere. During each subsequent time step the thickness is restored to its previous (original) value. The energy taken out of, or added to, the system locally (in order to maintain sea ice extent and thickness) is diagnosed from the change in surface energy budget. This approach is similar to applying a q-flux forcing to maintain sea ice in the sense that, as in simulations with the q-flux forcing, the analysis of prescribed sea ice simulations requires taking into account the imposed surface energy imbalance. However, applying the q-flux anomalies would make it difficult to obtain exactly the same sea ice thicknesses with different levels of CO_2 forcing. Prescribing the sea ice, on the other hand, allows an identical sea ice cover (extent and thickness) to be maintained regardless of CO_2 forcing. Prescribed ice setups, similar to the one in our study, have previously been employed by Ingram et al. (1989) and Rind et al. (1995).

Five additional simulations that parallel those described above (i.e., control (1 × CO_2) and 2, 4, 6 and 8 × CO_2) are performed for each of the zero and prescribed sea ice configurations. Anomalies for the active, zero, and prescribed sea ice simulations are determined relative to the 1 × CO_2 simulation with the same sea ice treatment. We focus on results from the 4 × CO_2 (quadrupled CO_2) simulations relative to the corresponding control simulations and further include the 2 × CO_2, 6 × CO_2, and 8 × CO_2 simulations to illustrate how our results scale with CO_2 concentration. The statistical significance of the response is determined using two-sided Student's *t* test. When comparing the anomalies due to increased CO_2 concentrations and different sea ice treatments we also consider their different control climates (at low CO_2 concentrations, the prescribed ice climate is similar to the active ice climate, while the zero ice climate is warmer). Analyzed monthly values represent 60 year climatological means, taken after the 30 year spin up.

3 Results

3.1 Global temperature response and climate sensitivity

Annual mean high latitude warming (4 × CO_2 − 1 × CO_2) in simulations with different sea ice treatments is shown in Fig. 1a–c. Arctic warming is most strongly pronounced in the active ice simulations (1a). In comparison, in the absence of sea ice response, in zero and prescribed ice simulations, high northern latitude warming is up to 10 K smaller (Figs. 1a–c, 2a, b). In the absence of sea ice changes, the strongest warming is over the land and not over the ocean as is the case in the active ice simulations.

Also shown in Fig. 1, are 0.15 and 0.9 autumn (SON) ice fractions from the 4 × CO_2 simulations (blue and white contour lines, respectively). In the active ice case, the Arctic is seasonally ice free (Fig. 1a). In the zero ice case, there is no sea ice present year round due to the experimental setup (Fig. 1b). In the prescribed ice simulation, the preindustrial sea ice cover is maintained (Fig. 1c).

Zonal temperature anomalies due to varying CO_2 levels from 1 × CO_2 to 2 ×, 4 ×, 6 × and 8 × CO_2 (Fig. 1d–f) further highlight the striking difference in temperature responses due to the different sea ice treatments. Whereas the most pronounced difference between the active ice and simulations with disabled ice response is in the high latitudes, low latitude warming also appears to be affected by the sea ice decline. For example, in the case of CO_2 quadrupling, ice response leads to an additional 1 to 2 K tropical temperature increase in active ice simulations relative to the zero and prescribed ice simulations (Figs. 1d–f, 2c, d).

Globally, mean temperature response to increasing CO_2 concentrations is larger in the active ice than in the zero and prescribed ice simulations (Fig. 3a, b). For the case of CO_2 quadrupling, global mean surface air temperature

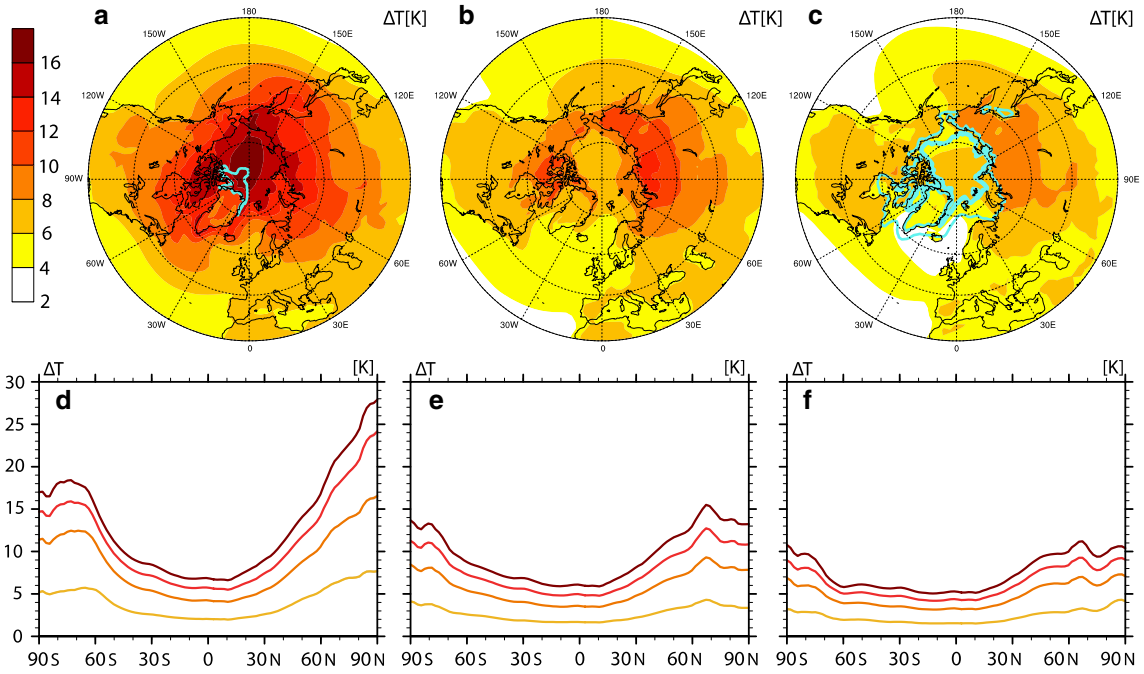

Fig. 1 High latitude annual mean (60°–90°N) and zonal annual mean surface air temperature anomalies. **a**–**c** Temperature responses to CO_2 quadrupling in simulations with active sea ice (**a**), no sea ice (zero ice treatment) (**b**) and prescribed ice (**c**) (all anomalies are statistically significant at the 95 % confidence level). *Blue* and *white contour lines* indicate 0.15 and 0.9 autumn (SON) ice fractions. In the active ice case (**a**) the Arctic is seasonally ice free, while in the prescribed ice simulation (**c**) the preindustrial sea ice cover is maintained. **d**–**f** Zonal temperature anomalies in 2 × CO_2 (*yellow*), 4 × CO_2 (*orange*), 6 × CO_2 (*red*) and 8 × CO_2 (*brown*) simulations relative 1 × CO_2, for active (**d**), zero (**e**) and prescribed (**f**) sea ice treatments. Standard errors (2σ-values) for all the values shown in panels **d**–**f** are smaller than 0.5 K

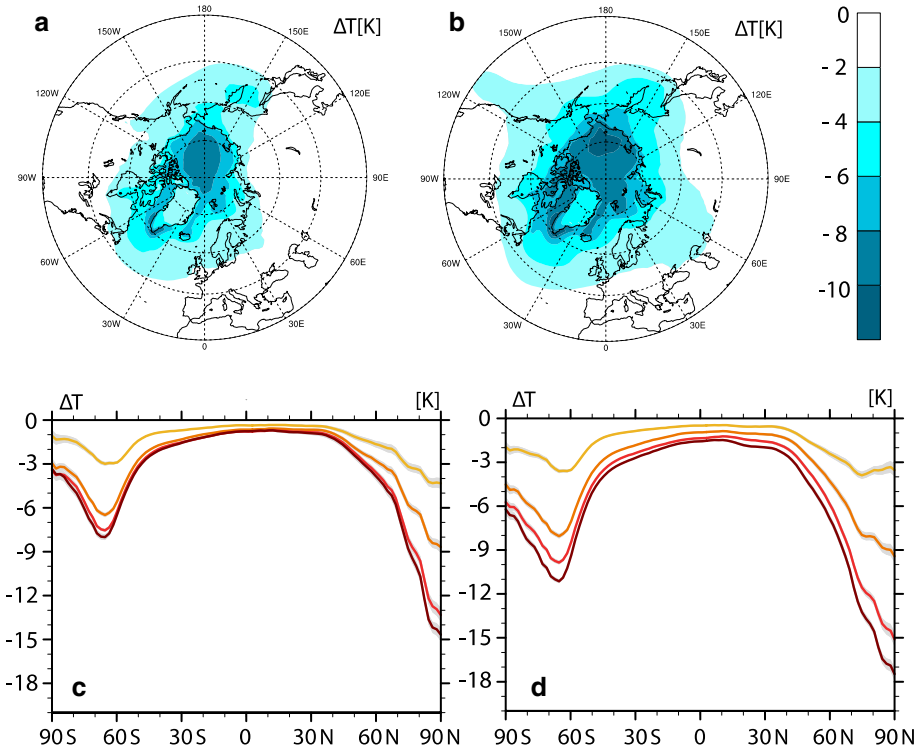

Fig. 2 Difference between the temperature responses in simulations with disabled sea ice changes relative to the active ice. *Upper plots* Annual mean surface air temperature anomalies (4 × CO_2 − 1 × CO_2) in zero ice relative to active ice ($\Delta T_z - \Delta T_a$) (**a**); and in prescribed ice relative to active ice treatment ($\Delta T_p - \Delta T_a$) (**c**). Anomalies shown are statistically significant at the 95 % confidence level. *Lower plots* zonal annual mean surface air temperature anomalies: 2 × CO_2 − 1 × CO_2 (*yellow*), 4 × CO_2 − 1 × CO_2 (*orange*), 6 × CO_2 − 1 × CO_2 (*red*) and 8 × CO_2 − 1 × CO_2 (*brown*) in zero ice relative to active ice simulations ($\Delta T_z - \Delta T_a$) (**c**) and in prescribed ice relative to active ice simulations ($\Delta T_p - \Delta T_a$) (**d**). Standard errors (2σ-values) are indicated with *grey shading*

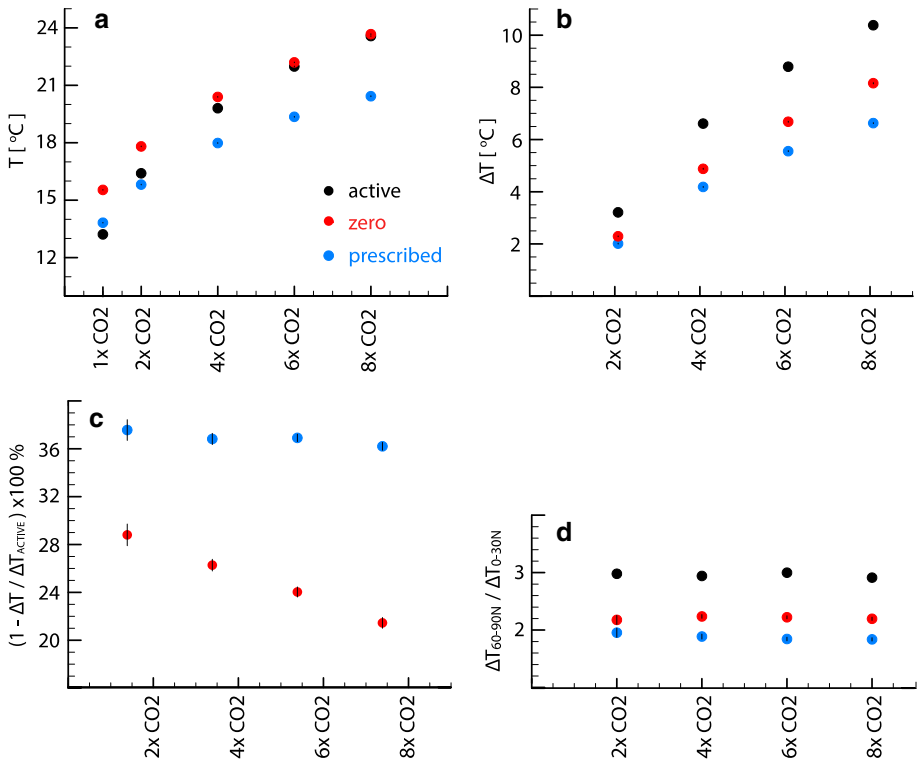

Fig. 3 The influence of active, zero and prescribed ice treatment on temperatures in 1 ×, 2 ×, 4 ×, 6 × and 8 × CO_2 simulations: **a** Global annual mean surface air temperatures [°C]; **b** global annual mean surface air temperature anomalies [°C]; **c** difference between the surface temperature responses in active and disabled ice simulations relative to the surface temperature response in active ice simulations (relative amount by which the global warming decreases in the absence of sea ice response, %); **d** high to low latitude warming ratio (surface temperature anomaly over the area 60°–90° N divided by the surface temperature anomaly over the area 0°–30°N). Corresponding standard errors (2σ-values) for all the points shown are smaller than: 0.03 K (**a**), 0.03 K (**b**), 1 % (**c**) and 0.08 (**d**)

changes equal 6.59 ± 0.03, 4.86 ± 0.02 and 4.16 ± 0.02 K in active, zero and prescribed ice simulations, respectively. Compared to the active ice simulations, zero ice simulations show smaller global temperature increase at low CO_2 concentrations (Fig. 3b). However, as the ice cover in active ice simulations disappears (with CO_2 increase), the difference between temperature response in active and zero ice simulations steadily decreases. In 2 × CO_2 simulations, temperature response with the zero ice treatment is 29 % smaller than with the active ice treatment, while in 8 × CO_2 simulations temperature response is 21 % smaller with zero ice relative to active ice treatment (Fig. 3c, red circles).

In simulations with the sea ice cover prescribed to pre-industrial values, the overall warming at any CO_2 level is ~37 % smaller than in the active ice simulations (Fig. 3c, blue circles). This near constancy of response with CO_2 level in the prescribed ice simulations is not particular to the 1 × CO_2 sea ice extent. Prescribing the 2 × CO_2 sea ice cover in the 4 ×, 6 × and 8 × CO_2 simulations yields 29 % less global mean temperature increase independently of CO_2 concentration (not shown).

The main cause of the different global temperature responses in zero and prescribed ice simulations is the surface energy imbalance imposed in the prescribed ice simulations while maintaining a constant sea ice extent. We illustrate this by considering the global annual mean top-of-atmosphere net flux anomalies ($\Delta \mathbf{N}_{TOA}$) plotted against the

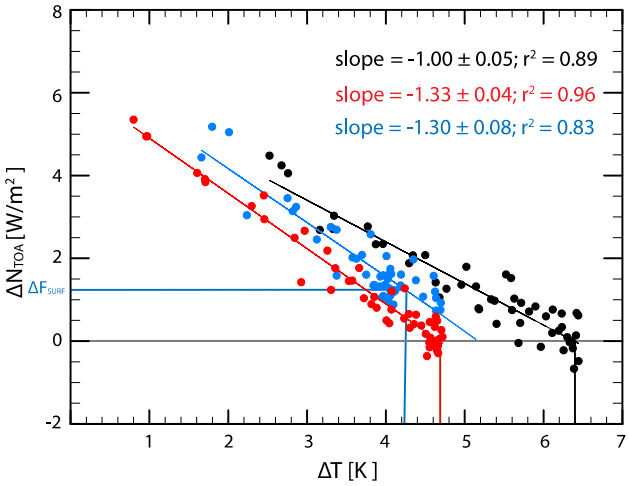

Fig. 4 Top-of-atmosphere net energy flux anomalies, $\Delta \mathbf{N}_{TOA}$, (W/m^2) (y-axis) plotted against the global mean surface air temperature anomalies, ΔT, (K) (x-axis) for CO_2 quadrupling simulations (*black* active ice, *red* zero ice, *blue* prescribed ice). *Points* shown represent the first 30 years of the model run and for each set of simulations (active, zero and prescribed), two additional ensemble members (spanning the first 10 years) have been added. Negative values of the regression coefficients for $\Delta \mathbf{N}_{TOA}$ against ΔT provide the values of the climate feedback parameters $\boldsymbol{\lambda}_a$, $\boldsymbol{\lambda}_z$ and $\boldsymbol{\lambda}_p$

global mean surface air temperature change (ΔT) for the case of CO_2 quadrupling (Fig. 4). This type of plot provides information on the initial top-of-atmosphere net energy

imbalance due to CO_2 quadrupling (y-axis intercept), the 'climate feedback parameter' λ (based on the value of the linear regression coefficient) and the equilibrium surface air temperature change (Gregory 2004). In Fig. 4 we consider the transient period only—plotted values span from year 1 till year 30 of the model simulation. In order to facilitate more accurate parameter determination, two additional CO_2 quadrupling simulations of a 10 year duration with slightly altered initial conditions are added for each set of simulations (active, zero and prescribed ice).

The atmosphere is in equilibrium when the top-of-the-atmosphere net energy budget equals the surface net energy budget. As in the active and zero ice simulations there is no imposed surface energy imbalance, global steady state temperature responses can be estimated from an intercept of the regression line and the $\Delta \mathbf{N}_{TOA} = 0$ W/m^2 line. In the prescribed ice 4 $\times$ CO_2 simulation, the imposed surface energy imbalance (relative to 1 $\times$ CO_2 prescribed ice simulation), $\Delta \mathbf{F}_{SURF}$, equals 1.24 $\pm$ 0.06 W/m^2. This is the energy removed in order to maintain the 1 $\times$ CO_2 sea ice extent in the 4 $\times$ CO_2 climate. The global temperature response is thus defined as the intercept of the regression line and the $\Delta \mathbf{N}_{TOA =}$ 1.24 W/m^2 line (that equals this surface net imbalance) and not the $\Delta \mathbf{N}_{TOA} = 0$ W/m^2 line. The intercept of the regression line and the $\Delta \mathbf{N}_{TOA} = 0$ W/m^2 line would lead to an incorrect estimate of the global temperature response in the 4 $\times$ CO_2 prescribed ice simulation (about 1 K higher).

The slopes of the regression lines in simulations with no sea ice response are similar and equal -1.33 ± 0.04 W/(m^2 K) and -1.38 ± 0.08 W/(m^2 K), for zero and prescribed ice simulations, respectively. Thus, the climate feedback parameters, λ_z and λ_p, are statistically indistinguishable between the prescribed and zero ice treatments. This further implies that the climate sensitivity (estimated as $1/\lambda$) is ~25 % smaller in simulations with disabled sea ice feedbacks relative to the simulation with active ice treatment [$\lambda_a = 1.00 \pm 0.05$ W/(m^2 K)]. However, the temperature responses between zero and prescribed ice simulations are different, due to the imposed surface forcing in the prescribed ice simulations. The global mean temperature increase due to CO_2 quadrupling in prescribed ice simulations is ~37 % smaller than the global mean temperature increase in the active ice simulation, while the same global mean temperature increase in the zero ice simulation is ~25 % of the corresponding active ice temperature increase (see Fig. 3b). Impacts of sea ice decline on global annual mean climate sensitivity and radiative forcing are discussed in greater detail in Caldeira and Cvijanovic (2014). However, due to a different sea ice prescription applied and different analytic approach used, values reported in Caldeira and Cvijanovic (2014) differ slightly from those presented here.

Finally, it is important to notice that different sea ice treatments have different control (1 $\times$ CO_2) climates (Fig. 3a). At low CO_2 levels, global mean surface air temperature in prescribed ice simulations is similar to the that in active ice simulation and both of these are cooler compared to the global mean temperature in the zero ice simulations. At higher CO_2 concentrations, active ice and zero ice simulations have similar global mean temperatures that are warmer than the corresponding global mean temperatures in the prescribed ice simulations. We take into account these different background climates when discussing the impacts of sea ice decline on global warming.

3.2 Equator-to-pole temperature gradient and atmospheric heat transport changes

Larger warming in high latitudes compared to the low latitudes (Fig. 1d–f) results in a decreased equator-to-pole temperature gradient. The largest weakening of the equator-to-pole gradient with CO_2 increase occurs in the active ice simulations. At low CO_2 concentrations, equator-to-pole temperature gradient in active ice simulations resembles the one in prescribed ice simulations. As the CO_2 concentrations increase, equator-to-pole temperature gradient in active ice simulations becomes similar to the gradient value from the zero ice simulations (not shown).

If we consider the ratio of surface warming over the area 60°–90°N and 0°–30°N, we observe that for any sea ice treatment this ratio is largely insensitive to the amount of global warming (Fig. 3d). In active ice simulations, Arctic warming is almost 3 times greater than tropical warming with the ratio changing from 2.91 $\pm$ 0.01 in the 2 $\times$ CO_2 simulation to 2.98 $\pm$ 0.04 in the 8 $\times$ CO_2 simulation. In the absence of sea ice changes, this ratio lies between 2.18 $\pm$ 0.08 and 2.24 $\pm$ 0.03 in zero ice and 1.95 $\pm$ 0.08 and 1.83 $\pm$ 0.03 in prescribed ice simulations, respectively. Thus, in the absence of sea ice response, both high and low latitude warming is weaker, with tropical changes being about half of the Arctic changes (in comparison to about one-third in the presence of a sea ice response).

Smaller changes in the high-to-low latitude temperature gradient in the absence of sea ice feedbacks may have an affect on the zonal flow and northward atmospheric heat transport (Jain et al. 1999; Cvijanovic et al. 2011; Karamperidou et al. 2012). Thus, we investigate if there is evidence that the sea ice loss is also leading to large-scale atmospheric circulation changes in our model simulations.

Atmospheric heat transport (AHT) anomalies (4 $\times$ CO_2 $-$ 1 $\times$ CO_2) and its dry static energy and LH transport components are shown in Fig. 5a. These anomalies are calculated from the atmospheric energy and fresh water budgets, assuming a steady state with constant (long

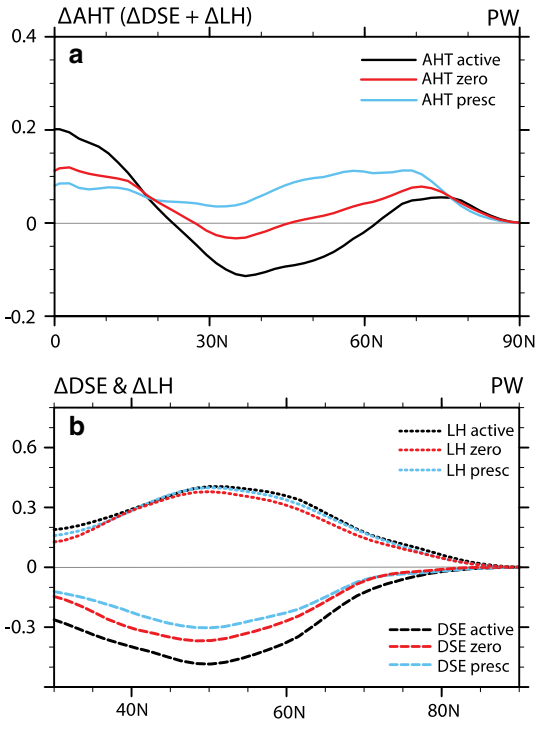

Fig. 5 **a** Northward atmospheric heat transport (AHT) anomalies (PW) in CO_2 quadrupling simulations and **b** mid- to high latitude northward AHT decomposition into latent (LH) and dry static energy (DSE) transports. *Black* active ice, *red* zero ice, *blue* prescribed ice. Standard errors (2σ-values) for all the anomalies shown are smaller than 0.01 PW

term) energy and moisture content in the atmospheric column, as described by Kay et al. (2012). This is a correct assumption for the multi-year averages used in our study.

In $4 \times CO_2$ relative to the $1 \times CO_2$ simulation, overall AHT increases for all sea ice treatments (Fig. 5a). This is a consequence of a large decrease in dry static energy (DSE) transport and smaller increase in LH transport (Fig. 5b). In the absence of sea ice response, midlatitude AHT changes are weaker than in the presence of sea ice changes. AHT decomposition, shown in Fig. 5b, indicates that this is mainly due to a weaker DSE transport increase, which ranges from largest in the active ice to smallest in the prescribed ice simulations. The relative magnitudes of DSE transport changes in active, zero and prescribed simulations are in accordance with the corresponding magnitudes of the equator-to-pole temperature gradient changes shown in Fig. 3d. In contrast, northward midlatitude LH transport response appears to be relatively insensitive of the sea ice changes.

In the tropics, AHT changes are largest in the active ice case. In accordance with the magnitude of their individual tropical AHT anomalies, tropical precipitation shifts are also most pronounced in the active ice simulations and weakest in the prescribed ice simulations (not shown). This is in line with the previous studies showing that the cross-equatorial AHT anomalies are associated with tropical precipitation shifts (Chiang and Bitz 2005; Kang et al. 2009; Cvijanovic and Chiang 2013).

3.3 Zonal wind responses and changes in extreme precipitation and temperature events

Annual mean 500 hPa zonal wind strength anomalies ($4 \times CO_2 - 1 \times CO_2$) obtained with different sea ice treatments are shown in Fig. 6a–c. In the active ice simulation, zonal westerly wind flow weakens over most of the northern midlatitudes (Fig. 6a). This is in agreement with other studies finding a weakening of the zonal westerly flow in response to enhanced Arctic warming and decreased mid- to high latitude geopotential thickness gradient (Francis et al. 2009; Overland and Wang 2010; Francis and Vavrus 2012). In contrast, in the prescribed and zero ice simulations, westerly flow increases in strength in the upper midlatitudes, especially over the North Atlantic and northern Europe (Fig. 6b, c). Similar responses are also detected in the upper level flow (300 hPa) (not shown). Analysis of seasonal means shows that different 500 hPa zonal wind responses observed in annual means are most pronounced in the Northern Hemisphere winter (DJF) and fall (SON). Figure 6, panels d–f, shows the 500 hPa zonal wind changes for the winter DJF season. Strengthening of the zonal wind flow is larger in the prescribed ice than in the zero ice simulations. The difference between the DJF zonal wind strength changes in simulations with and without sea ice response is illustrated in Fig. 7. Zonal wind strength anomalies in zero ice simulations relative to the active ice simulations (Fig. 7a) are smaller than the corresponding anomalies between the prescribed ice and active ice simulations (Fig. 7b). This is in accordance with the smaller difference in the amount of high latitude warming between the zero ice and active ice simulations (Fig. 2a) and the prescribed ice and active ice simulations (Fig. 2b), consistent with the thermal wind balance.

Different westerly wind responses to CO_2 induced warming in the presence or absence of sea ice changes (Fig. 6) may have an impact on extreme weather development in the northern midlatitudes. Previous study by Francis and Vavrus (2012) suggested that the weakened zonal winds and slower progression of upper-level waves could lead to an increase in extreme weather events as a result of prolonged conditions. Similarly, Peings and Magnusdottir (2014) found that Arctic amplification and reduced midlatitude westerlies favor the increased intensity of cold extremes over certain midlatitude regions. Moreover, since the midlatitude dry static energy transport is maintained by eddies, different DSE transport responses in simulations with active and disabled sea ice response (see Sect. 3.2)

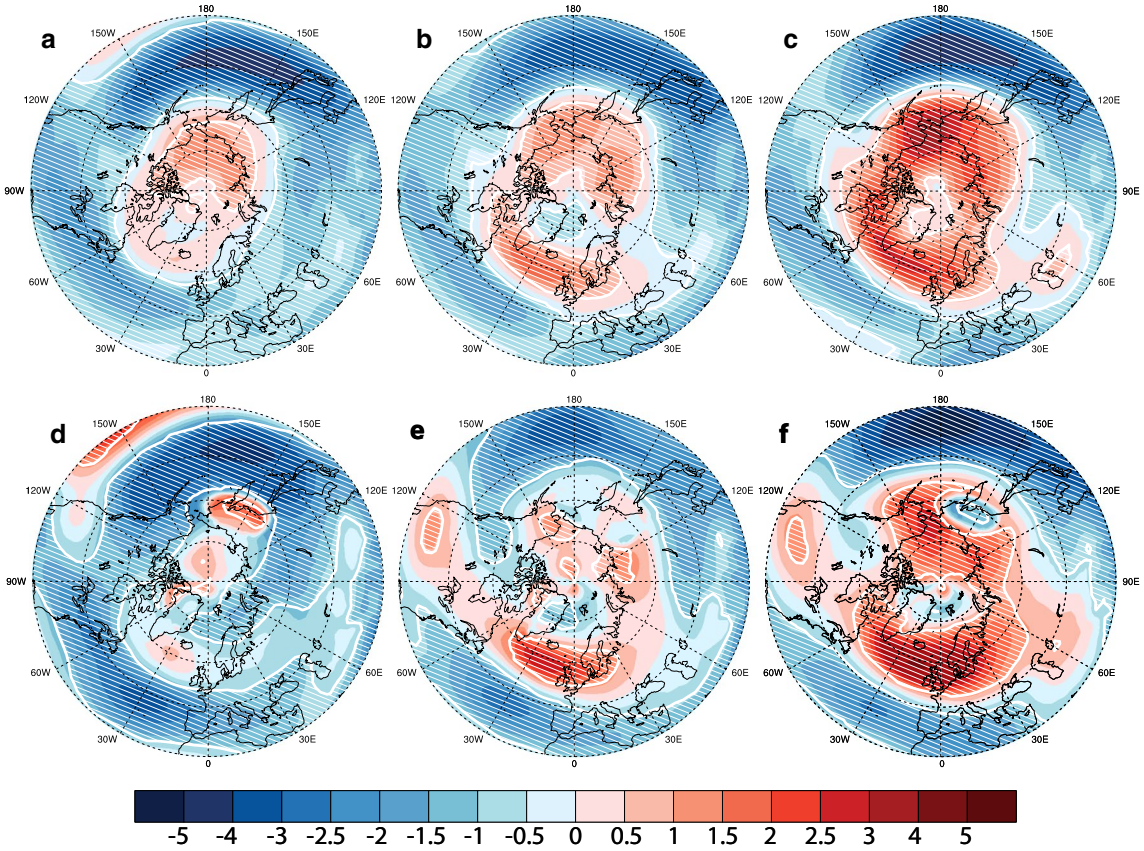

Fig. 6 Annual (**a**–**c**) and DJF (**d**–**f**) 500 hPa zonal wind strength anomalies ΔU (m/s) in 4 × CO_2 relative to 1 × CO_2 simulations: **a**, **d** active ice, **b**, **e** zero ice and **c**, **f** prescribed ice. *White dashed areas* indicate the anomalies that are statistically significant at the 95 % confidence level

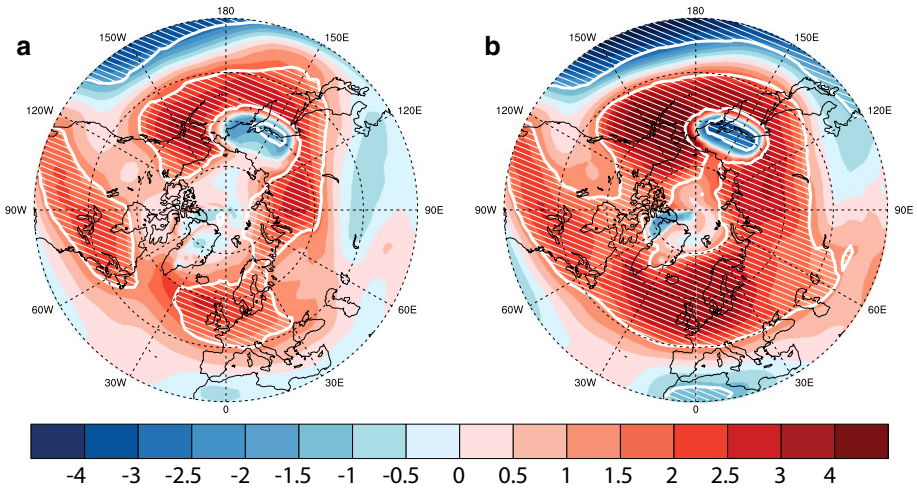

Fig. 7 Difference between the wind responses in simulations with disabled sea ice changes relative to the active ice treatment. **a** DJF 500 hPa zonal wind anomalies (m/s) (4 × CO_2 − 1 × CO_2) in zero relative to active ice treatment ($\Delta U_z - \Delta U_a$); and **b** in prescribed relative to active ice treatment ($\Delta U_p - \Delta U_a$). *White dashed areas* indicate the anomalies that are statistically significant at the 95 % confidence level

may be another indicator of sea ice response affecting the atmospheric circulation patterns in the midlatitudes. We thus continue our analysis by comparing the strengths and frequencies of various extreme weather indices under different sea ice treatments. The indices considered are the maximum precipitation over a given period, the number of heavy precipitation days, the minimum temperature over a given period and the number of frost days (as described in Sillmann et al. 2013). These indices are evaluated from a total of 30 years of daily data. The analysis is limited to the winter (DJF) season as this is the season with the largest impact of sea ice treatment on zonal wind strengths. Values

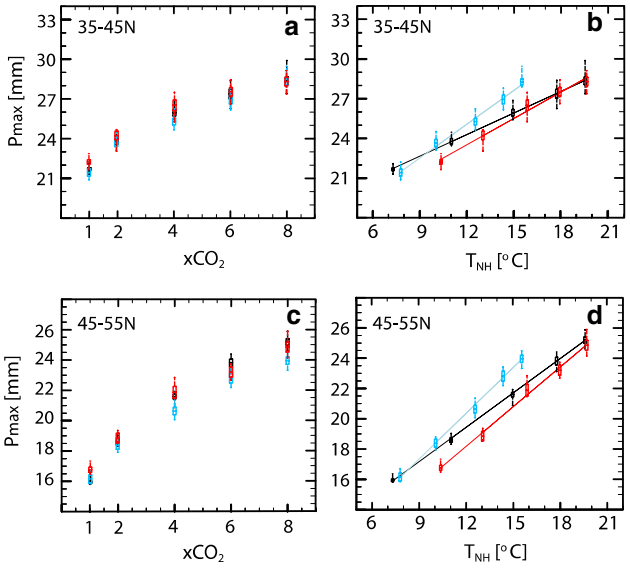

Fig. 8 Winter (DJF) precipitation maxima P_{max} (mm) relative to the CO_2 level (**a**, **c**) and Northern Hemispheric DJF surface air temperature [°C] (**b**, **d**). *Boxes* median with one standar error; *whiskers* interquartile range. **a**, **b** Averages over the 35°N–45°N latitude band and **c**, **d** over the 45°–55°N latitude band ("lower" and "upper" midlatitudes). *Colors* refer to different sea ice treatments: *black* active, *red* zero, *blue* prescribed ice. *Lines* are to guide the eye only

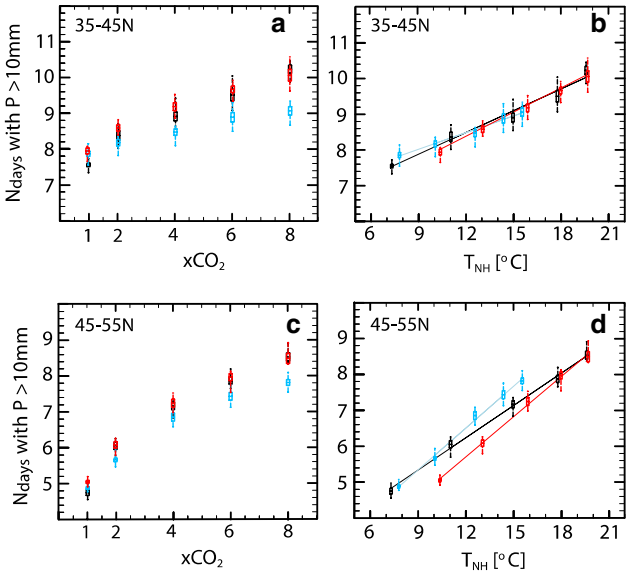

Fig. 9 Number of heavy DJF precipitation events (P > 10 mm) [−] relative to CO_2 level (**a**, **c**) and Northern Hemispheric DJF surface air temperature [°C] (**b**, **d**). *Boxes* median with one standard error; *whiskers* interquartile range. **a**, **b** Averages over the 35°N–45°N latitude band and **c**, **d** over the 45°–55°N latitude band ("lower" and "upper" midlatitudes). *Colors* refer to different sea ice treatments: *black* active, *red* zero, *blue* prescribed ice. *Lines* are to guide the eye only

of all the indices are first estimated at a given grid-cell and then averaged over the "lower" (35°–45°N) and "upper" (45°–55°N) midlatitude bands.

We first consider the change in the intensity of the winter precipitation maxima (P_{max}). For each DJF season in the 30 year period, we select the day with the largest amount of precipitation (Fig. 8). In all simulations, independent of sea ice treatment, we see an increase in the precipitation maxima with an increase in CO_2 concentration (Fig. 8 panels a and c). At a given CO_2 level, the differences between simulations with different sea ice treatment are not statistically significant. In order to account for different background states in simulations with different sea ice treatments, precipitation maxima are also plotted relative to the DJF northern hemispheric surface air temperature (Fig. 8 panels b and d). At a given temperature, prescribed ice simulations show higher winter precipitation maxima relative to the zero ice simulations (both in the lower and upper midlatitudes). In the active ice simulations, precipitation maxima tend to resemble the prescribed ice simulations at lower temperatures and zero ice simulations at higher temperatures. Overall, P_{max} appears to be less sensitive to NH temperature increase in simulations featuring larger equator-to-pole gradient changes (active ice) than in the simulations featuring smaller equator-to-pole gradient changes (zero and prescribed ice).

Next we consider the impacts of sea ice response on the frequency of heavy DJF precipitation events (defined as the number of days within a season with total precipitation larger than 10 mm). This is illustrated in Fig. 9, showing the number of DJF heavy precipitation events relative to: the CO_2 level (panels a and c) and the hemispheric mean DJF temperature (panels b and d). In the lower midlatitudes, at high CO_2 concentrations, prescribed ice simulations show a lower number of heavy precipitation events compared to zero or active ice simulations (Fig. 9a). However, sea ice treatment appears not to affect the number of heavy precipitation events after taking into account different NH temperature responses in the active, zero and prescribed ice simulations (Fig. 9b). Thus, in the lower midlatitudes, the hemispheric temperature change appears to be a very good indicator of the number of heavy precipitation events for any sea ice treatment. As shown earlier, global (and hemispheric) temperatures are influenced by the sea ice changes; the relative impact of sea ice changes due to increased CO_2 concentrations accounts for 21–37 % of the overall CO_2 induced warming in our model simulations (Fig. 3c). A notable difference in warming between the simulations with and without sea ice responses is required in order to achieve a substantial (and statistically significant) difference in the number of heavy precipitation events. This

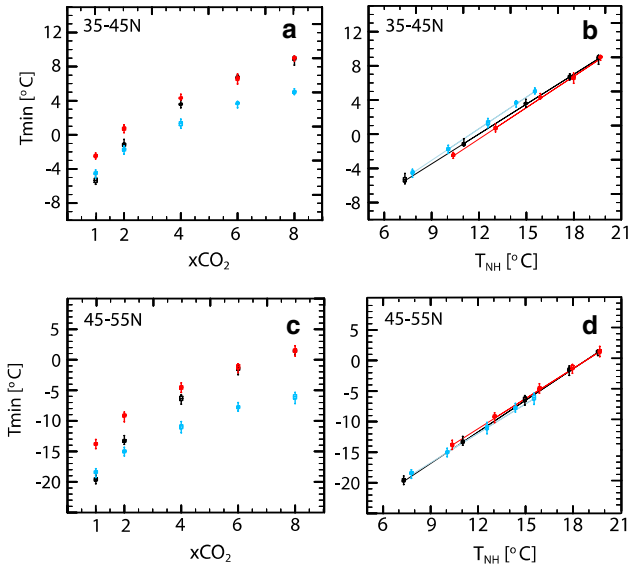

Fig. 10 As in Figs. 8 and 9 but for winter (DJF) temperature minima T_{min} [°C]

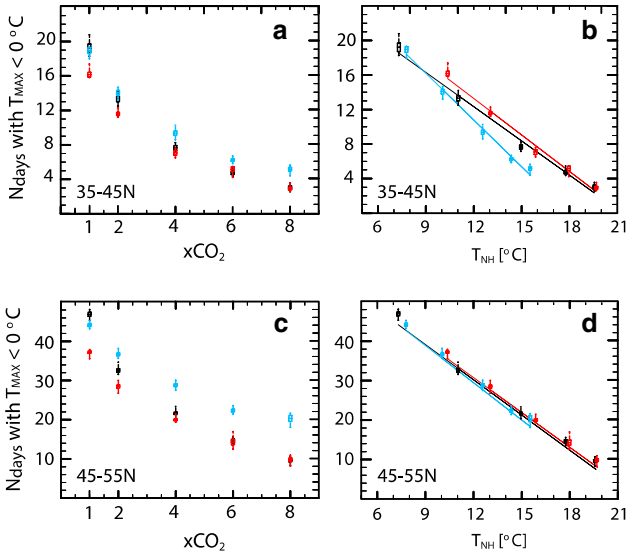

Fig. 11 As in Figs. 8 and 9 but for the number of ice days (number of days with maximum daily temperature below 0 °C) [−]

is satisfied for large CO_2 forcing (e.g., in Fig. 9a this is achieved at 8 × CO_2 concentration).

In the upper midlatitudes, simulations with different sea ice treatments also show a statistically different number of heavy precipitation events only at high CO_2 concentrations (Fig. 9c). At a given northern hemispheric DJF temperature, prescribed ice simulations have more heavy precipitation days than the zero ice simulations, while the number of heavy precipitation events in the active ice simulations resembles that in the prescribed ice simulations at lower temperatures and that in the zero ice simulations at higher temperatures (Fig. 9d). Similarly as before, we find the simulations featuring smaller equator-to-pole gradient change (prescribed and zero ice simulations) to be more sensitive to NH temperature increase than the simulations featuring larger equator-to-pole gradient change (active ice simulations).

Changes in winter temperature minima and the number of ice days are shown in Figs. 10 and 11, respectively. Winter temperature minima increases with CO_2 concentration in all simulations, both in lower and upper midlatitudes, while different sea ice treatments result in different responses in T_{min}. Winter temperature minima are larger in zero ice than in prescribed ice simulations, while the active ice simulations minima are located between these two (Fig. 10a, c). When considering T_{min} relative to the corresponding northern hemispheric DJF temperature (Fig. 10b, d) differences between the sea ice treatments are mostly not present. Northern hemispheric DJF temperature thus appears to be a very good indicator of the grid-cell scale change in winter temperature minima. However, it is important to recall that hemispheric temperatures are affected by the sea ice treatment. Different responses in T_{min} originating from the different sea ice treatments are eliminated when taking into account different NH temperature responses in active, zero and prescribed ice treatment.

The number of ice days in DJF season decreases with increasing CO_2 concentration across the midlatitude sector (Fig. 11a, c). Prescribed ice simulations feature a larger number of ice days than the zero ice simulation, in agreement with the weaker global temperature increase in prescribed ice simulations. The number of ice days in the active ice simulations falls in between the zero ice and prescribed ice simulations. Considered at a given temperature, over the lower midlatitude sector prescribed ice simulations have a lower number of ice days than zero ice simulations (Fig. 11b). The decrease in the number of ice days with NH temperature is larger in prescribed and zero than in the active ice simulations. In the upper midlatitudes, simulations with different ice treatments show the same response to hemispheric temperature increase (Fig. 11d).

4 Discussion

In this study we attempt to isolate the sea ice loss driven component of global warming by analyzing the difference between simulations with active and disabled sea ice treatment. We focus on the impacts of sea ice decline on global temperature increase, midlatitude atmospheric circulation changes and extreme weather events.

In a set of idealized simulations in which the pre-industrial sea ice cover is maintained despite global warming, we

find the temperature response to be 37 % smaller than in the presence of sea ice loss (independent of CO_2 concentrations). In a companion paper (Caldeira and Cvijanovic 2014) this number is somewhat smaller as a consequence of different sea ice extents used in prescribed ice simulations (here we use 30 years of monthly sea ice data instead of 1 year). In another set of idealized simulations, in which the oceans are allowed to super-cool without forming the sea ice, we find 29, 26, 24 and 21 % less global warming in 2, 4, 6 and 8 × CO_2 simulations, respectively, than in the simulations with the active ice treatment (Fig. 3).

Our *prescribed ice* treatment is very similar to that applied in the studies by Ingram et al. (1989) and Rind et al. (1995). Rind et al. (1995) estimated the sea ice loss to account for 37 % of global surface air temperature increase in CO_2-doubling simulations, while Ingram et al. (1989) had a lower estimate of 19 %. While our findings are in close agreement with Rind et al. (1995), the differences between our findings and those of Ingram et al. (1989) are most likely due to inter-model differences. It is important to highlight that our estimates include any feedbacks related to sea ice changes (ice albedo, ice insulation) and also other feedbacks triggered by sea ice response (for example, cloud or water vapor changes).

The concept behind the prescribed ice simulations presented here is to ensure that the sea ice area and thickness do not change as the climate warms. In contrast, in zero ice simulations all sea ice properties are 'eliminated' from the system: there is no sea ice albedo feedback, atmosphere–ocean insulation effect, nor any effects related to phase transitions, snow accumulation or thermal properties of the ice surface compared to the ocean surface that is allowed to super-cool. While the zero ice and prescribed ice treatments may seem very different, our analysis reveals that they actually have the same values of the climate feedback parameter λ (Fig. 4), which, for the case of CO_2 quadrupling, is ~25 % larger compared to the one obtained with the active ice treatment.

In the absence of sea ice loss, we find a weaker amplification of high latitude warming, but also less tropical warming. This remote temperature effect of sea loss is in agreement with the previous findings of Meehl and Washington (1990), Rind et al. (1995) and Hall (2004). We also find weaker tropical precipitation changes in the absence of sea ice changes, implying that the differences in simulated sea ice responses are a likely contributing factor to inter-model differences in predicted tropical precipitation responses with global warming.

In our active ice simulations, sea ice loss affects midlatitude upper level flow, leading to a decrease in midlatitude zonal wind strengths with global warming. In contrast, in the absence of sea decline, zonal westerly wind flow in the upper midlatitudes strengthens with increasing CO_2 concentrations. The largest impact of sea ice treatment (presence or absence of sea ice response) on zonal wind strengths is found in the winter (DJF) season over the North Atlantic and Western Europe (Figs. 6, 7).

Our model simulations indicate that sea ice cover affects extreme precipitation and temperature events across the midlatitude sector in the winter. At a given high CO_2 concentration, three out of four considered indices (number of heavy precipitation events, number of ice days and the winter temperature minima) show a dependence on sea ice treatment (Figs. 9, 10, 11). In the case of the number of heavy precipitation events (Fig. 9), this dependence is weak and detectable only at very high CO_2 concentrations (i.e., 8 × CO_2). In some cases (e.g., for the number of heavy precipitation events in the lower mildatitudes, winter temperature minima and the number of ice days in the upper midlatitudes), the difference due to the sea ice treatment can be eliminated when taking into account the effect that the absence or presence of sea ice response has on the global (and/or hemispheric) mean temperatures. In other cases (number of ice days in the lower midlatitudes, number of heavy precipitation events in the upper midlatitudes) taking into account hemispheric temperatures reveals an additional, weaker and opposing effect than the one expected from the global temperature increase. For example, in the lower midlatitudes, at a given CO_2 concentration, prescribed ice simulations show a *higher* number of ice days than zero ice simulations. However, considered at a given hemispheric temperature, prescribed ice simulations have a *lower* number of ice days than zero ice simulations. The sensitivity of these indices to hemispheric temperature change is weakest in simulations with the largest equator-to-pole temperature gradient changes (active ice) and strongest in simulations with the smallest equator-to-pole temperature gradient changes (prescribed and zero ice simulations). Finally, in the case of winter precipitation maxima, different responses were found only when comparing different sea ice treatments at a given temperature and not at a given CO_2 level (Fig. 8).

While in our study we find the meridional temperature gradient change to be a useful factor in describing the dependence of extreme events on sea ice treatment, our analysis does not imply causation between the equator-to-pole temperature gradient and extreme events, thus opening an avenue for future exploration. Equator–to-pole temperature gradient changes can influence the jet stream, total eddy transport of sensible heat in winter as well as the baroclinicity (Lorenz 1984, Jain et al. 1999, Karamperidou et al. 2012), all of which are factors that may have an impact on the midlatitude weather patterns. Moreover, different responses of midlatitude dry static energy transport (shown in Fig. 5) in our simulations are consistent with the corresponding equator-to-pole gradient changes.

5 Conclusions

Recent dramatic sea ice decline, accompanied by model predictions of a seasonally ice free Arctic in the near future, have raised questions regarding the possible remote effects and consequences of these abrupt high latitude changes. As the global temperature continues to rise, the intensity and the frequency of heavy precipitation events is expected to increase (Meehl et al. 2007, 2012). Sea ice decline, as a major amplifier of global warming, may have the potential to affect the development of extreme precipitation events in the future.

The links between sea ice decline and extreme cold events have been widely hypothesized. A number of studies suggest that recent Arctic sea ice decline has lead to an increased likelihood of extreme cold events in winter over NH continents (Honda et al. 2009; Petoukhov and Semenov 2010; Overland and Wang 2010; Liu et al. 2012; Peings and Magnusdottir 2014). While there is a growing amount of evidence linking the Arctic amplification with midlatitude atmospheric circulation changes (Overland and Wang 2010; Francis and Vavrus 2012; Screen et al. 2013), there are also large uncertainties in understanding the mechanism of midlatitude response to Arctic sea ice loss (Screen and Simmonds 2013; Barnes 2013). Motivated by this, we investigated the overall impacts of sea ice decline on global warming in simulations with active and disabled sea ice response.

In the absence of sea ice feedbacks, we find weaker global warming and decreased climate sensitivity to CO_2 forcing. The weakening of warming has a global signature, although it is most pronounced over the polar regions. Furthermore, we find that presence (or absence) of sea ice cover affects midlatitude zonal winds as well as strength and frequency of midlatitude extreme weather events (temperature minima, number of days with heavy precipitation and number of ice days) during the DJF season.

Sea ice decline affects a wide range of climatically important quantities, including the mean hemispheric temperature and equator-to-pole temperature gradient. Our results suggest that a comprehensive understanding of the role of sea ice on extreme events in the midlatitudes will depend on deepening our understanding of how the sea ice decline induced amplification of hemispheric warming and decreased meridional temperature gradients affect midlatitudes weather systems.

Observational studies are not yet able to determine whether the impact of extreme ice loss on extreme weather is strong enough to be distinguished from natural variability (Kattsov et al. 2010; Kay et al. 2011; Hopsch et al. 2012), while most global climate models are overly conservative in their sea ice projections (Serreze et al. 2007; Stroeve et al. 2012, Wang and Overland 2013). Thus, the approach described in this study may represent a valuable tool for separating the consequences of sea ice loss in global warming simulations. We encourage the development of similar approaches that could further address this topic by, for example, including the effects of deep ocean changes as well as investigating extreme weather changes in model simulations with higher spatial resolution.

References

Alexeev VA, Jackson CH (2012) Polar amplification: is atmospheric heat transport important? Clim Dyn 41(2):533–547. doi:10.1007/s00382-012-1601-z

Alexeev VA, Langen PL, Bates JR (2005) Polar amplification of surface warming on an aquaplanet in "ghost forcing" experiments without sea ice feedbacks. Clim Dyn 24(7–8):655–666. doi:10.1007/s00382-005-0018-3

Barnes EA (2013) Revisiting the evidence linking Arctic Amplification to extreme weather in midlatitudes. Geophys Res Lett. doi:10.1002/grl.50880

Blüthgen J, Gerdes R, Werner M (2012) Atmospheric response to the extreme Arctic sea ice conditions in 2007. Geophys Res Lett 39:L02707. doi:10.1029/2011gl050486

Broccoli AJ, Dahl KA, Stouffer RJ (2006) Response of the ITCZ to Northern Hemisphere cooling. Geophys Res Lett. doi:10.1029/2005gl024546

Budyko MI (1969) The effect of solar radiation variations on the climate of the Earth. Tellus 21(5):611–619. doi:10.1111/j.2153-3490.1969.tb00466.x

Caldeira K, Cvijanovic I (2014) Estimating the contribution of sea ice response to climate sensitivity in a climate model. J Clim 27:8597–8607. doi:10.1175/JCLI-D-14-00042.1

Chapman WL, Walsh JE (2007) Simulations of arctic temperature and pressure by global coupled models. J Clim 20(4):609–632. doi:10.1175/jcli4026.1

Chiang JCH, Bitz CM (2005) Influence of high latitude ice cover on the marine Intertropical Convergence Zone. Clim Dyn 25(5):477–496. doi:10.1007/s00382-005-0040-5

Cvijanovic I, Chiang JCH (2013) Global energy budget changes to high latitude North Atlantic cooling and the tropical ITCZ response. Clim Dyn 40(5–6):1435–1452. doi:10.1007/s00382-012-1482-1

Cvijanovic I, Langen PL, Kaas E (2011) Weakened atmospheric energy transport feedback in cold glacial climates. Clim Past 7(4):1061–1073. doi:10.5194/cp-7-1061-2011

Cvijanovic I, Langen PL, Kaas E, Ditlevsen PD (2013) Southward Intertropical Convergence Zone shifts and implications for an Atmospheric Bipolar Seesaw. J Clim 26(12):4121–4137. doi:10.1175/jcli-d-12-00279.1

Danabasoglu G, Gent PR (2009) Equilibrium climate sensitivity: is it accurate to use a slab ocean model? J Clim 22(9):2494–2499. doi:10.1175/2008jcli2596.1

Deser C, Tomas R, Alexander M, Lawrence D (2010) The seasonal atmospheric response to projected arctic sea ice loss in the late twenty-first century. J Clim 23(2):333–351. doi:10.1175/2009jcli3053.1

Ding Q, Wallace JM, Battisti DS, Steig EJ, Gallant AJE, Kim H-J, Geng L (2014) Tropical forcing of the recent rapid

Arctic warming in northeastern Canada and Greenland. Nature 509(7499):209–212
Francis JA, Vavrus SJ (2012) Evidence linking Arctic amplification to extreme weather in midlatitudes. Geophys Res Lett 39:L06801. doi:10.1029/2012gl051000
Francis JA, Chan W, Leathers DJ, Miller JR, Veron DE (2009) Winter Northern Hemisphere weather patterns remember summer Arctic sea-ice extent. Geophys Res Lett. doi:10.1029/2009gl037274
Gent PR, Danabasoglu G, Donner LJ, Holland MM, Hunke EC, Jayne SR, Lawrence DM, Neale RB, Rasch PJ, Vertenstein M, Worley PH, Yang Z-L, Zhang M (2011) The Community Climate System Model Version 4. J Clim 24(19):4973–4991. doi:10.1175/2011jcli4083.1
Graversen RG, Wang M (2009) Polar amplification in a coupled climate model with locked albedo. Clim Dyn 33(5):629–643. doi:10.1007/s00382-009-0535-6
Graversen RG, Mauritsen T, Tjernström M, Källén E, Svensson G (2008) Vertical structure of recent Arctic warming. Nature 451(7174):53–56. doi:10.1038/nature06502
Gregory JM (2004) A new method for diagnosing radiative forcing and climate sensitivity. Geophys Res Lett. doi:10.1029/2003gl018747
Hall A (2004) The role of surface albedo feedback in climate. J Clim 17(7):1550–1568. doi:10.1175/1520-0442(2004)017<1550:trosaf>2.0.co;2
Hansen J, Lacis A, Rind D, Russell G, Stone P, Fung I, Ruedy R, Lerner J (1984) Climate sensitivity: analysis of feedback mechanisms 29:130–163. doi:10.1029/GM029p0130
Holland MM, Bitz CM (2003) Polar amplification of climate change in coupled models. Clim Dyn 21(3–4):221–232. doi:10.1007/s00382-003-0332-6
Holland MM, Bitz CM, Weaver AJ (2001) The influence of sea ice physics on simulations of climate change. J Geophys Res 106(C9):19639. doi:10.1029/2000jc000651
Holland MM, Bitz CM, Hunke EC, Lipscomb WH, Schramm JL (2006a) Influence of the sea ice thickness distribution on polar climate in CCSM3. J Clim 19(11):2398–2414. doi:10.1175/jcli3751.1
Holland MM, Bitz CM, Tremblay B (2006b) Future abrupt reductions in the summer Arctic sea ice. Geophys Res Lett. doi:10.1029/2006gl028024
Honda M, Inoue J, Yamane S (2009) Influence of low Arctic sea-ice minima on anomalously cold Eurasian winters. Geophys Res Lett. doi:10.1029/2008gl037079
Hopsch S, Cohen J, Dethloff K (2012) Analysis of a link between fall Arctic sea ice concentration and atmospheric patterns in the following winter. Tellus A. doi:10.3402/tellusa.v64i0.18624
Hsieh WC, Collins WD, Liu Y, Chiang JCH, Shie CL, Caldeira K, Cao L (2013) Climate response due to carbonaceous aerosols and aerosol-induced SST effects in NCAR community atmospheric model CAM3.5. Atmos Chem Phys 13(15):7489–7510. doi:10.5194/acp-13-7489-2013
Hunke EC, Lipscomb WH (2008) CICE: The Los Alamos sea ice model user's manual, version 4
Ingram WJ, Wilson CA, Mitchell JFB (1989) Modeling climate change: an assessment of sea ice and surface albedo feedbacks. J Geophys Res 94(D6):8609. doi:10.1029/JD094iD06p08609
IPCC (2007) Climate Change 2007: The Physical Science Basis. Cambridge
Jackson JM, Carmack EC, McLaughlin FA, Allen SE, Ingram RG (2010) Identification, characterization, and change of the near-surface temperature maximum in the Canada Basin, 1993–2008. J Geophys Res. doi:10.1029/2009jc005265
Jain S, Lall U, Mann ME (1999) Seasonality and interannual variations of North Hemisphere temperature: equator-topole gradient and ocean–land contrast. J Clim 12:1086–1100
Kang SM, Frierson DMW, Held IM (2009) The tropical response to extratropical thermal forcing in an idealized GCM: the importance of radiative feedbacks and convective parameterization. J Atmos Sci 66(9):2812–2827. doi:10.1175/2009jas2924.1
Kapsch M-L, Graversen RG, Tjernström M (2013) Springtime atmospheric energy transport and the control of Arctic summer sea-ice extent. Nat Clim Change 3(8):744–748. doi:10.1038/nclimate1884
Karamperidou C, Cioffi F, Lall U (2012) Surface temperature gradients as diagnostic indicators of mid-latitude circulation dynamics. J Clim 25:4154–4171. doi:10.1175/JCLI-D-11-00067.1
Kattsov VM, Ryabinin VE, Overland JE, Serreze MC, Visbeck M, Walsh JE, Meier W, Zhang X (2010) Arctic sea-ice change: a grand challenge of climate science. J Glaciol 56(200):1115–1121. doi:10.3189/002214311796406176
Kay JE, Holland MM, Jahn A (2011) Inter-annual to multi-decadal Arctic sea ice extent trends in a warming world. Geophys Res Lett 38:L15708. doi:10.1029/2011gl048008
Kay JE, Holland MM, Bitz C, Blanchard-Wrigglesworth E, Gettelman A, Conley A, Bailey D (2012) The influence of local feedbacks and northward heat transport on the equilibrium Arctic climate response to increased greenhouse gas forcing. J Clim 25:5433–5450
Langen PL, Alexeev VA (2007) Polar amplification as a preferred response in an idealized aquaplanet GCM. Clim Dyn 29(2–3):305–317. doi:10.1007/s00382-006-0221-x
Lawrence DM, Oleson KW, Flanner MG, Thornton PE, Swenson SC, Lawrence PJ, Zeng X, Yang Z-L, Levis S, Sakaguchi K, Bonan GB, Slater AG (2011) Parameterization improvements and functional and structural advances in version 4 of the Community Land Model. J Adv Model Earth Syst. doi:10.1029/2011ms000045
Liu J, Curry JA, Wang H, Song M, Horton RM (2012) Impact of declining Arctic sea ice on winter snowfall. Proc Natl Acad Sci. doi:10.1073/pnas.1114910109
Lorenz EN (1984) Irregularity: a fundamental property of the atmosphere. Tellus 36A:98–100
Mahlstein I, Knutti R (2011) Ocean heat transport as a cause for model uncertainty in projected arctic warming. J Clim 24(5):1451–1460. doi:10.1175/2010jcli3713.1
Manabe S, Stouffer RJ (1980) Sensitivity of a global climate model to an increase of CO_2 concentration in the atmosphere. J Geophys Res 85(C10):5529. doi:10.1029/JC085iC10p05529
Masson-Delmotte V, Kageyama M, Braconnot P, Charbit S, Krinner G, Ritz C, Guilyardi E, Jouzel J, Abe-Ouchi A, Crucifix M, Gladstone RM, Hewitt CD, Kitoh A, LeGrande AN, Marti O, Merkel U, Motoi T, Ohgaito R, Otto-Bliesner B, Peltier WR, Ross I, Valdes PJ, Vettoretti G, Weber SL, Wolk F, Yu Y (2005) Past and future polar amplification of climate change: climate model intercomparisons and ice-core constraints. Clim Dyn 26(5):513–529. doi:10.1007/s00382-005-0081-9
Meehl GA, Washington WM (1990) CO_2 climate sensitivity and snow-sea-ice albedo parameterization in an atmospheric GCM coupled to a mixed-layer ocean model. Clim Change 16, doi:10.1007/BF00144505
Meehl GA, Stocker TF, Collins WD, Friedlingstein P, Gaye AT, Gregory JM, Kitoh A, Knutti R, Murphy JM, Noda A, Raper SCB, Watterson IG, Weaver AJ, Zhao Z-C (2007) Clim Change. The Physical Science Basis. Contribution of Working Group I to the Fourth Assessment Report of the Intergovernmental Panel on Climate Change
Meehl GA, Washington WM, Arblaster JM, Hu A, Teng H, Tebaldi C, Sanderson BN, Lamarque J-F, Conley A, Strand WG, White JB (2012) Climate system response to external forcings and climate change projections in CCSM4. J Clim 25(11):3661–3683. doi:10.1175/jcli-d-11-00240.1

Murray C, Walsh J (2005) A model ensemble assessment of the enhancement of arctic warming by sea ice retreat. Sola 1:57–60. doi:10.2151/sola.2005-016

National Snow and Ice Data Center (2012) Arctic sea ice news and Analysis. http://nsidc.org/arcticseaicenews/2012/09/arctic-sea-ice-extent-settles-at-record-seasonal-minimum/. Accessed 19 Sept 2012

Neale RB, Richter J, Park S, Lauritzen PH, Vavrus SJ, Rasch PJ, Zhang M (2013) The mean climate of the community atmosphere model (CAM4) in forced SST and Fully coupled experiments. J Clim 26(14):5150–5168. doi:10.1175/jcli-d-12-00236.1

Overland JE, Wang M (2010) Large-scale atmospheric circulation changes are associated with the recent loss of Arctic sea ice. Tellus A 62(1):1–9. doi:10.1111/j.1600-0870.2009.00421.x

Overland JE, Wood KR, Wang M (2011) Warm Arctic-cold continents: climate impacts of the newly open Arctic Sea. Polar Res. doi:10.3402/polar.v30i0.15787

Peings Y, Magnusdottir G (2014) Response of the Wintertime Northern Hemisphere atmospheric circulation to current and projected arctic sea ice decline: a numerical study with CAM5. J Clim 27:244–264. doi:10.1175/JCLI-D-13-00272.1

Petoukhov V, Semenov VA (2010) A link between reduced Barents–Kara sea ice and cold winter extremes over northern continents. J Geophys Res. doi:10.1029/2009jd013568

Polyakov IV (2005) One more step toward a warmer Arctic. Geophys Res Lett. doi:10.1029/2005gl023740

Rind D, Healy R, Parkinson C, Martinson D (1995) The role of sea ice in 2 × CO_2 climate model sensitivity. part I: the total influence of sea ice thickness and extent. J Clim 8(3):449–463. doi:10.1175/1520-0442(1995)008<0449:trosii>2.0.co;2

Robock A (1983) Ice and snow feedbacks and the latitudinal and seasonal distribution of climate sensitivity. J Atmos Sci 40(4):986–997. doi:10.1175/1520-0469(1983)040<0986:iasfat>2.0.co;2

Screen JA (2013) Influence of Arctic sea ice on European summer precipitation. Environ Res Lett 8:044015. doi:10.1088/1748-9326/8/4/044015

Screen JA, Simmonds I (2010) The central role of diminishing sea ice in recent Arctic temperature amplification. Nature 464(7293):1334–1337. doi:10.1038/nature09051

Screen JA, Simmonds I (2013) Exploring links between Arctic amplification and midlatitude weather. Geophys Res Lett 40(5):959–964. doi:10.1002/grl.50174

Screen JA, Simmonds I, Deser C, Tomas R (2013) The atmospheric response to three decades of observed arctic sea ice loss. J Clim 26(4):1230–1248. doi:10.1175/jcli-d-12-00063.1

Sellers WD (1969) A global climatic model based on the energy balance of the earth-atmosphere system. J Appl Meteorol 8(3):392–400. doi:10.1175/1520-0450(1969)008<0392:agcmbo>2.0.co;2

Serreze MC, Francis JA (2006) The Arctic amplification debate. Clim Change 76(3–4):241–264. doi:10.1007/s10584-005-9017-y

Serreze MC, Holland MM, Stroeve J (2007) Perspectives on the Arctic's Shrinking Sea-Ice cover. Science 315(5818):1533–1536. doi:10.1126/science.1139426

Serreze MC, Barrett AP, Stroeve JC, Kindig DN, Holland MM (2009) The emergence of surface-based Arctic amplification. The Cryosphere 3(1):11–19. doi:10.5194/tc-3-11-2009

Sillmann J, Kharin VV, Zhang X, Zwiers FW, Bronaugh D (2013) Climate extremes indices in the CMIP5 multimodel ensemble: part 1 Model evaluation in the present climate. J Geophys Res Atmos 118(4):1716–1733. doi:10.1002/jgrd.50203

Solomon A (2006) Impact of latent heat release on polar climate. Geophys Res Lett. doi:10.1029/2005gl025607

Stroeve JC, Serreze MC, Holland MM, Kay JE, Malanik J, Barrett AP (2011) The Arctic's rapidly shrinking sea ice cover: a research synthesis. Clim Change 110(3–4):1005–1027. doi:10.1007/s10584-011-0101-1

Stroeve JC, Kattsov V, Barrett A, Serreze M, Pavlova T, Holland M, Meier WN (2012) Trends in Arctic sea ice extent from CMIP5, CMIP3 and observations. Geophys Res Lett 39:L16502. doi:10.1029/2012gl052676

Vavrus SJ, Harrison SP (2003) The impact of sea-ice dynamics on the Arctic climate system. Clim Dyn 20(7–8):741–757. doi:10.1007/s00382-003-0309-5

Wang M, Overland JE (2012) A sea ice free summer Arctic within 30 years: An update from CMIP5 models. Geophys Res Lett 39:L18501. doi:10.1029/2012gl052868

Wang M, Overland JE (2013) When will the summer Arctic be nearly sea ice free? Geophys Res Lett 40:2097–2101. doi:10.1002/grl.50316

Washington WM, Meehl GA (1996) High-latitude climate change in a global coupled ocean-atmosphere-sea ice model with increased atmospheric CO2. J Geophys Res 101(D8):12795. doi:10.1029/96jd00505